NASA TECHNICAL NOTE

NASA TN D-3096

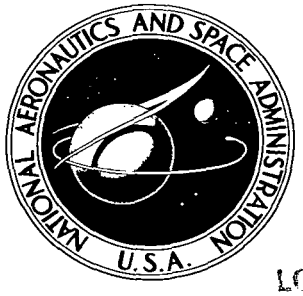

EXPERIMENTAL STUDY OF END EFFECT AND PRESSURE PATTERNS IN HELICAL GROOVE FLUID FILM SEAL (VISCOSEAL)

by Lawrence P. Ludwig, Thomas N. Strom, and Gordon P. Allen

Lewis Research Center
Cleveland, Ohio

NATIONAL AERONAUTICS AND SPACE ADMINISTRATION • WASHINGTON, D. C. • NOVEMBER 1965

EXPERIMENTAL STUDY OF END EFFECT AND PRESSURE PATTERNS IN HELICAL GROOVE FLUID FILM SEAL (VISCOSEAL)

By Lawrence P. Ludwig, Thomas N. Strom, and Gordon P. Allen

Lewis Research Center
Cleveland, Ohio

NATIONAL AERONAUTICS AND SPACE ADMINISTRATION

For sale by the Clearinghouse for Federal Scientific and Technical Information
Springfield, Virginia 22151 – Price $1.00

EXPERIMENTAL STUDY OF END EFFECT AND PRESSURE PATTERNS IN HELICAL GROOVE FLUID FILM SEAL (VISCOSEAL)

by Lawrence P. Ludwig, Thomas N. Strom, and Gordon P. Allen

Lewis Research Center

SUMMARY

An experimental investigation was conducted on the pressure patterns in a viscoseal consisting of a smooth rotor and a stationary helically grooved housing. The sealed fluid was a mineral oil, and the investigation was within the laminar-flow regime (maximum Reynolds number of 300). Results indicated that when the grooves communicated directly with the pressurized cavity, an end effect, or ineffective seal length, was evidenced by a sharp decay of pressure along the land leading edge. This end effect was eliminated by incorporating a short dam which blocked direct communication of the groove with the pressurized cavity. Measurements of pressure patterns within the viscoseal confirmed existing theoretical predictions of linear pressure gradients and disclosed a method of applying the theoretical pressure generation equation to determine wetted-seal length.

INTRODUCTION

Those designs of rotating machinery for generation of electrical power in outer space which utilize shaft seals have two basic requirements, high seal reliability for 1 to 3 years of unattended operation and seal leakage rates of less than several pounds per year, because of inventory limits (ref. 1) or contamination. For these operating requirements the helical groove fluid film seal (hereinafter called the viscoseal) is a promising device which has inherent long life and high reliability because of the absence of solid surfaces in sliding contact. For example, it is potentially useful for sealing turbine loop fluids (condensed vapors of alkali metals to 1800° R) employed in the Rankine cycle electric power generation system (ref. 2).

The helical groove type of geometry was first used in pumping applications, and a pump exhibited by Sir John Dewrance in 1920 was capable of a pressure generation of

689 Newtons per square centimeter (1000 lb/sq in.). Interest in this pump led to the development of mathematical theories which were published in 1922 and 1928 (refs. 3 to 5). Helical groove pump devices used in the extrusion of plastics were covered by a series of papers (refs. 6 to 12) which treats the extrusion laminar flow process, pressure generation, and power absorption both theoretically and experimentally.

In a paper of major significance, Boon and Tal (ref. 13) developed a viscoseal theory based on laminar flow. Their analysis included flow components neglected by others and provided optimization of the geometries for maximum sealing capacity and minimum power absorption.

Theoretical and experimental results for the laminar-flow regime have been published by several authors (refs. 14 to 16). Experimental results for the turbulent-flow regime with water and oils as test fluids were reported in reference 14.

Several authors (refs. 16 and 17) reported that the viscoseal had a certain ineffective length at the high-pressure end of the seal. This has been called the end effect, and it has been suggested (ref. 16) that this ineffective rotor length be subtracted from the calculated wetted-seal length in order to compare theory and experiment. Muijderman (ref. 18) derived theoretical pressure patterns for the spiral groove geometry on plane surfaces and developed an analytical method of correcting for the end effect. However, pressure patterns in the viscoseal and end-effect alterations of these patterns have not been determined experimentally. Existing experimental data consist of average pressure measurements (refs. 16 and 17) from which the existence of an end effect is deduced. End-effect, or ineffective lengths Z_i, ranging from 1.340 centimeters (0.528 in.) to 0.304 centimeter (0.120 in.) have been reported (refs. 16 and 17, respectively). Lengths of these magnitudes are of considerable practical importance in the application of the viscoseal to machinery in which length and weight are restricted.

The objective of this program is to study the pressure patterns in the viscoseal with particular emphasis on the pattern near the seal end (end effect). These studies employ a viscoseal having internal helical grooves in a stationary housing. Since, in the laminar-flow regime, there is no difference between the sealing action of grooves in the housing and that of grooves on a rotating shaft, the stationary grooves in the housing were chosen in the interest of more convenient instrumentation. A mineral oil was used as the test fluid, and the operating speeds provided studies in the laminar-flow regime to a maximum Reynolds number of 300.

VISCOSEAL CONCEPTS

The three basic combinations of viscoseals (all having relative motion between shaft and housing) are

(1) Smooth shaft and helically grooved housing (fig. 1(a))

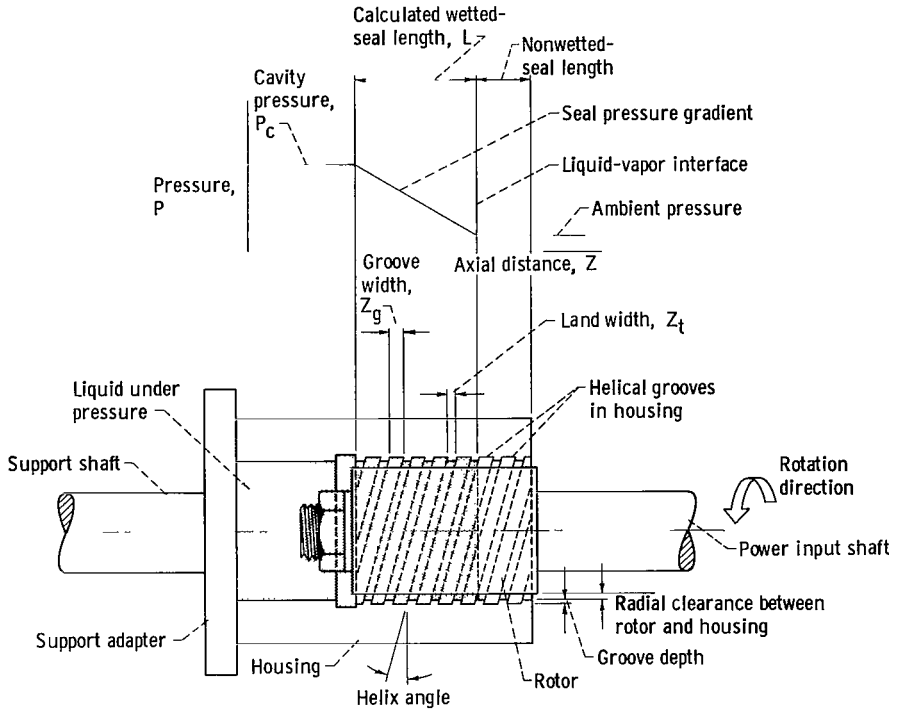

(a) Smooth rotor and housing with helical grooves.

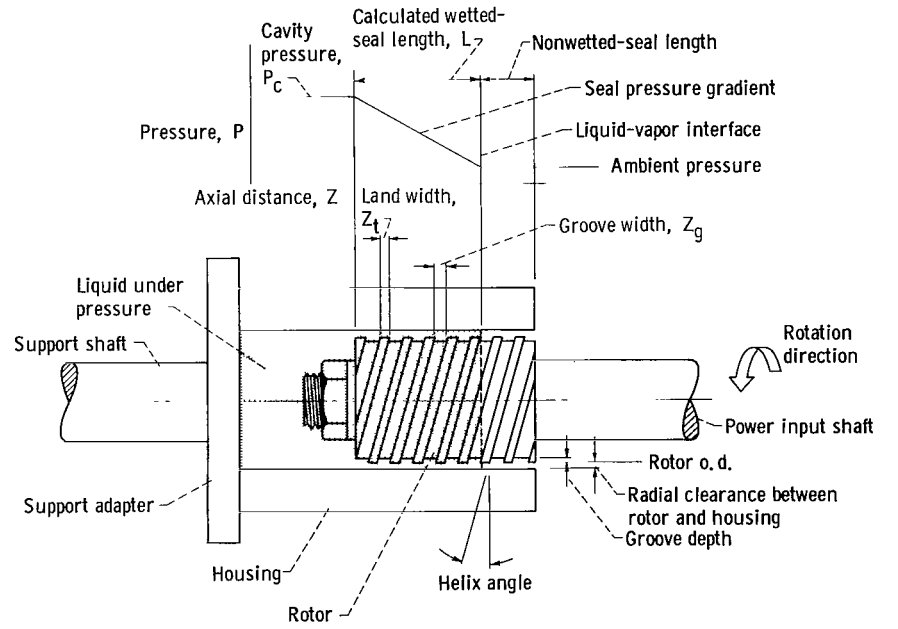

(b) Helically grooved shaft and smooth-bore housing.

Figure 1. - Viscoseal elements.

(2) Helically grooved shaft and smooth bore housing (fig. 1(b))

(3) Helically grooved shaft and helically grooved housing

The relative rotation of the shaft (rotor) within the housing tends to pump the liquid, by viscous drag, back into the cavity, and a sealing condition is established when the fluid is pumped back as fast as it tends to leak out. Therefore, a liquid-vapor interface is established under sealing conditions (see fig. 1(a)), and a pressure gradient is developed from the ambient pressure at the interface to the cavity pressure (high-pressure end).

The theory for the viscoseal is based on a full fluid film in the annulus formed by the rotor and the housing. The thickness of this fluid film is much smaller than the circumferential and axial lengths. Therefore, the theoretical problem can be reduced to one in which the rotational motion is replaced by translational motion, and the cube in figure 2 represents an infinitesimal fluid particle in this film. Through application of Newton's second law of motion, the component forces on the fluid particle are equated to the mass and component accelerations to yield the Navier-Stokes equations (ref. 19):

$$\rho \frac{Du}{dt} = \rho f_x + \frac{\partial}{\partial x} \sigma_x + \frac{\partial}{\partial y} \tau_{xy} + \frac{\partial}{\partial z} \tau_{xz}$$

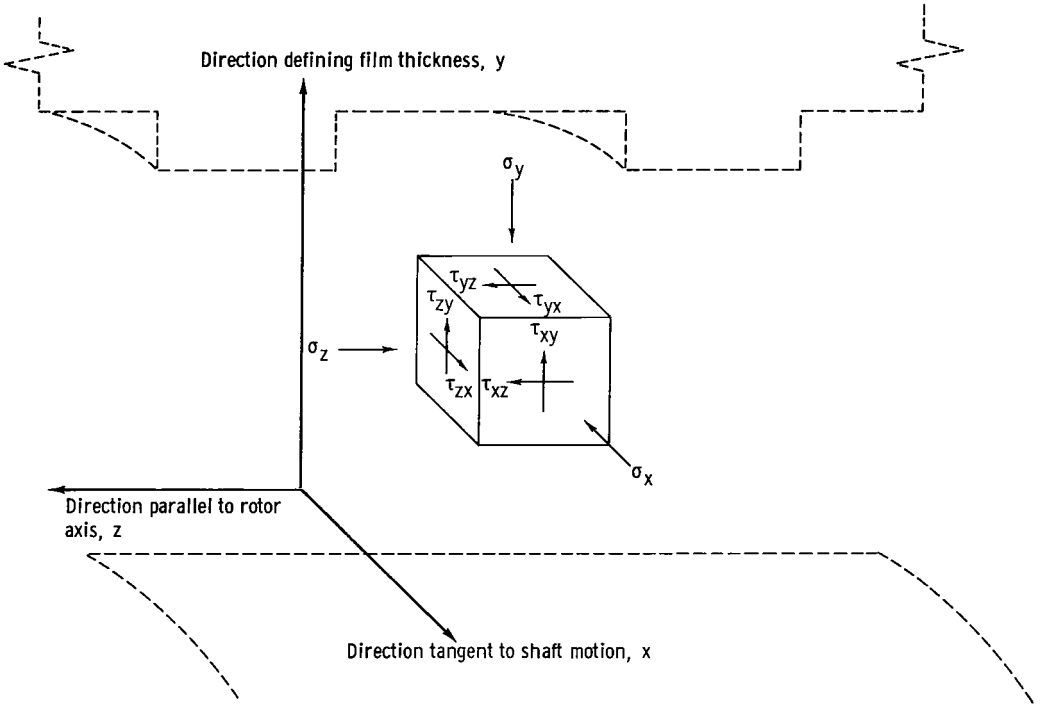

Figure 2. - Normal force component, σ; shear force component τ; velocity components in x-, y-, and z-directions, respectively, u, v, and w. Infinitesimal fluid particle in viscoseal fluid film.

$$\rho \frac{Dv}{dt} = \rho f_y + \frac{\partial}{\partial x} \tau_{xy} + \frac{\partial}{\partial y} \sigma_y + \frac{\partial}{\partial z} \tau_{yz}$$

$$\rho \frac{Dw}{dt} = \rho f_z + \frac{\partial}{\partial x} \tau_{xz} + \frac{\partial}{\partial y} \tau_{yz} + \frac{\partial}{\partial z} \sigma_z$$

where ρ is the unit mass density, u, v, and w are velocity components in the x-, y-, and z-direction, respectively, t is time, and f_x, f_y, and f_z are external force components per unit mass. The normal force components on the cube faces σ_x, σ_y, and σ_z are equal to

$$\sigma_x = - P - \frac{2}{3}\mu\left(\frac{\partial u}{\partial x} + \frac{\partial v}{\partial y} + \frac{\partial w}{\partial z}\right) + 2\mu \frac{\partial u}{\partial x}$$

$$\sigma_y = - P - \frac{2}{3}\mu\left(\frac{\partial u}{\partial x} + \frac{\partial v}{\partial y} + \frac{\partial w}{\partial z}\right) + 2\mu \frac{\partial v}{\partial y}$$

$$\sigma_z = - P - \frac{2}{3}\mu\left(\frac{\partial u}{\partial x} + \frac{\partial v}{\partial y} + \frac{\partial w}{\partial z}\right) + 2\mu \frac{\partial w}{\partial z}$$

The shear force components on the cube faces τ_{xy}, τ_{yx}, τ_{xz}, τ_{zx}, τ_{yz}, and τ_{zy} are equal to

$$\tau_{xy} = \tau_{yx} = \mu\left(\frac{\partial u}{\partial y} + \frac{\partial v}{\partial x}\right)$$

$$\tau_{xz} = \tau_{zx} = \mu\left(\frac{\partial u}{\partial z} + \frac{\partial w}{\partial x}\right)$$

$$\tau_{yz} = \tau_{zy} = \mu\left(\frac{\partial v}{\partial z} + \frac{\partial w}{\partial y}\right)$$

In application to the viscoseal, the Navier-Stokes equations for laminar flow can be considerably simplified, without significant error, by the following assumptions:

(1) There is no variation in pressure P in the direction defining film thickness; therefore,

$$\frac{\partial P}{\partial y} = 0$$

(2) No external forces act on the film; therefore,

$$f_x = f_y = f_z = 0$$

(3) The fluid shear forces are large compared to the fluid inertia forces; hence

$$\frac{Du}{dt} = \frac{Dv}{dt} = \frac{Dw}{dt} = 0$$

(4) All velocity gradients are negligible when compared to $\partial u/\partial y$ and $\partial w/\partial y$

These preceeding assumptions eliminate from consideration the Navier-Stokes equation for the y-direction, and equations for the x- and z-directions are reduced to

$$\frac{1}{\mu}\frac{\partial P}{\partial x} = \frac{\partial^2 u}{\partial y^2}$$

$$\frac{1}{\mu}\frac{\partial P}{\partial z} = \frac{\partial^2 w}{\partial y^2}$$

Several authors (refs. 13 to 16) have derived the viscoseal pressure generation capacity by applying these equations, which result from simplification of the Navier-Stokes equations, to the viscoseal geometry. There is general agreement that the form of the pressure generation equation is

$$P = \frac{6\mu ULG}{c^2}$$

where

P pressure at high-pressure end of seal

μ absolute viscosity

U rotor peripheral velocity

L calculated wetted-seal length

G function of helical geometry, dimensionless

c radial clearance

TABLE I. - COMPARISONS OF THE GEOMETRY FACTOR G

Reference	Formula for G	Calculated optimum groove geometry			Optimum G
		$r = \frac{Z_g}{Z_g + Z_t}$	$s = \frac{c + h}{c}$	$f = \tan \ell$	
	(a)				
13	$\frac{fr(1 - r)(s - 1)\left(s^3 - 1\right)}{\left(1 + f^2\right)s^3 + f^2 r(1 - r)\left(s^3 - 1\right)^2}$	0.50	3.65	0.281	0.0912
14	$\frac{m^2(1 + m)^{-1}}{f\left[1 + \frac{Em^3}{r(1 - r)\sin^2 \ell}\right]}$ where E = 1 to 2.5	0.50	3.78	0.395	0.1018 (E = 1)
15	$\frac{1}{(Q + 1)\left[1 + (4Q + 1)m\right]\left\{\frac{1 - 0.630}{m^2} + \left[\frac{48n(1/r)^2}{Q \sin \ell}\right]\right\}}$ where $n = 0.00531\left(\frac{Z_t}{c}\right)^{-0.75}$	0.63	4.12	0.250	0.1160
20	$\frac{\left(s^3 - 1\right)(s - 1)\sin 2(90 - \ell)}{\left(1 - s^3\right)^2 + 2s^3\left[1 + \left(\frac{Z_g}{Z_t}\right)^2\right]\frac{Z_t}{Z_g} + \left(s^3 - 1\right)^2 \cos 2(90 - \ell)}$	0.50	3.61	0.244	0.0912

[a]Radial clearance, c; eccentricity factor, E; helix angle, ℓ; groove depth, h; groove width, Z_g; land width, Z_t; $m = c/h$; $Q = h/Z_g$.

Although there is agreement on the form of the equation, significant differences exist in the derived expression for G; table I lists these expressions and the corresponding optimum groove ratios.

By theory (ref. 13) the pressure generation capacity of both viscoseal arrangements (see fig. 1) are identical for the usual helical seal geometries. Also, for pressure generation, it is immaterial which element, shaft or housing, is rotating; however, practical differences may exist in the leakage tendency because of inertial forces, seal orientation, and surface energy forces.

APPARATUS AND PROCEDURE

Figure 3 shows a schematic drawing of the experimental apparatus and viscoseal assembly. The rotor of the viscoseal is attached to the power input shaft, which is

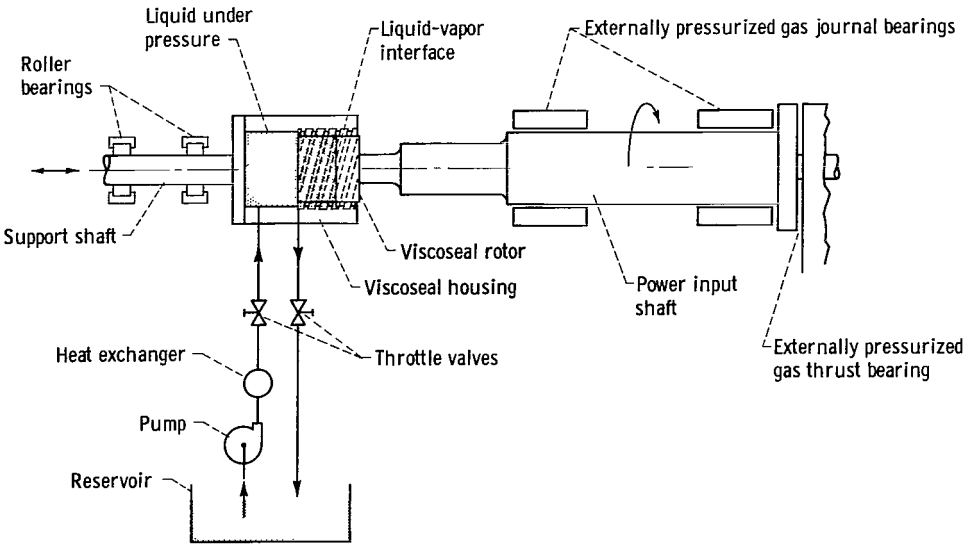

Figure 3. - Viscoseal and hydraulic system.

supported by externally pressurized gas journal bearings. Axial thrust due to sealed fluid cavity pressure against the rotor is resisted by the externally pressurized gas thrust bearing. The power input shaft is driven by a variable-speed electric drive and step-up transmission. A magnetic pickup monitors the shaft speed. The viscoseal housing is attached to a support shaft and roller bearing assembly, which permits axial adjustment. A pump pressurizes the seal housing cavity and circulates a cooling fluid flow from the reservoir, through a heat exchanger, to the test cavity and then back to the reservoir. This cooling flow is necessary to control fluid film temperature in the viscoseal. The steel rotors have a centerline average surface finish of 0.5 micron (20 μin.) and are mounted within 0.00508 centimeter (0.0002 in.) of the total indicator reading. The viscoseal housing is constructed from acrylic plastic and contains thermocouples and pressure taps as shown in figure 4.

Pressure taps, in a line parallel to the axis, are located at groove edges and midland and midgroove positions; pressure taps are also located near both edges along one groove. Two sets of four pressure taps (90° apart) were used to aline the housing with respect to the rotor within 0.0102 centimeter (0.0004 in.) as determined by calibration. Thermocouples were located flush with the bore and groove root in a line parallel to the axis and at each midgroove and midland position.

Figure 4 also gives the groove dimensions used in this evaluation. The housing had a 5.082-centimeter (2.001-in.) bore and a $14\frac{1}{2}^{\circ}$ helix angle. Groove widths of 0.48 centimeter (0.19 in.) and land widths of 0.33 centimeter (0.13 in.) were provided by using five helix grooves (five starts). These geometric porportions, which are based on the optimum relations given by reference 15, included a 0.038 centimeter (0.015 in.) groove depth and a rotor radial clearance of 0.0127 centimeter (0.005 in.).

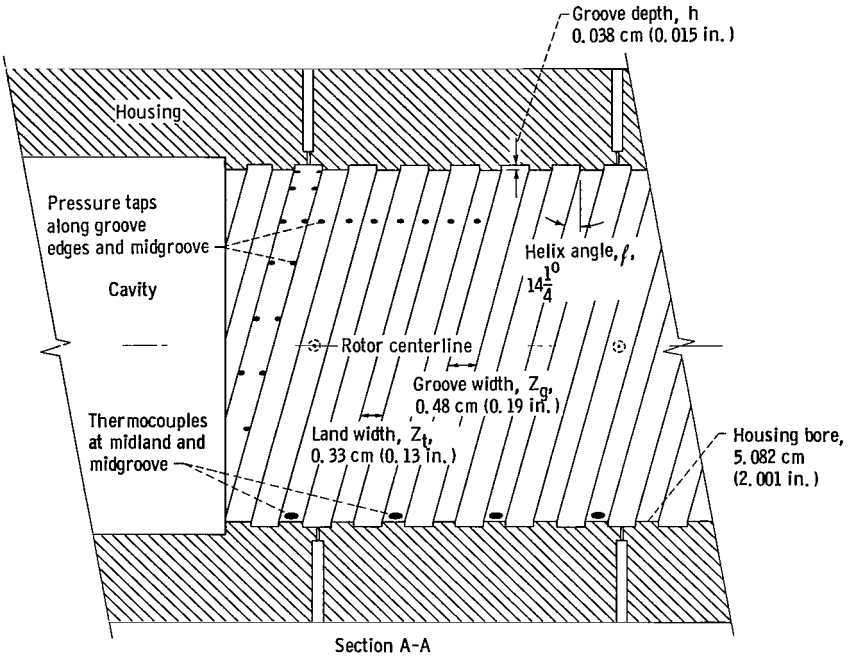

(a) Axial locations.

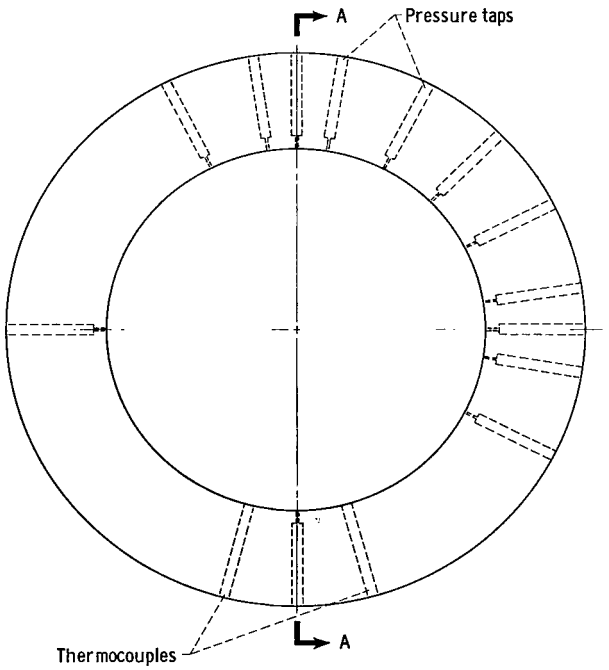

(b) Circumferential locations.

Figure 4. - Pressure tap and thermocouple locations.

TABLE II. - VISCOSITY OF MINERAL OIL

Temperature		Viscosity, cs
^{o}F	^{o}C	
100	37.8	71.2
130	54.4	32.4
210	98.9	8.4

The viscosity-temperature relations for the mineral oil used were found to be the same before and after use in the test. These values can be found in table II.

RESULTS AND DISCUSSION

Figure 5 shows an experimentally determined pressure pattern in a viscoseal composed of an internal helically grooved housing and a smooth rotor arrangement, like that illustrated in figure 1(a). In a plane orthogonal to the rotor centerline, the pressure increases across the groove (from point A to B) in the direction of rotor rotation and decreases across the land (from point B to C). The increase and decrease in pressure repeat for each groove-land pair and produce a saw-tooth pressure profile in the orthogonal plane. The pressure increases from the low-pressure end (plane 3) to the high-pressure end (plane 1), and the pressure pattern has a helical twist corresponding to the helical grooves.

The pressure gradients in the planes orthogonal to the rotor centerline are essentially linear for axial positions not influenced by the end effects. Evidence of this linear gradient is given in figure 6, which shows typical experimental results. These pressure profiles are the same as those for the orthogonal planes shown in figure 5 except that a single groove-land pair is unwrapped to form a plane figure. (Neglecting curvature is not a significant error since the ratio of rotor radius to groove depth is 65 to 1.)

In these orthogonal planes, the ratio of pressure to cavity pressure P/P_c increases linearly over the groove and then decreases linearly over the land. This linear relation was found to hold to the maximum test speed of 6000 rpm, which produced a Reynolds number of 300 in the grooves. This saw-tooth pressure pattern agrees with the theoretical development given by Muijderman (ref. 18).

End Effect

When the helical grooves communicate directly with the pressurized cavity, the pressure developed along the land leading edge decays sharply near the high-pressure end of the seal. Typical results are shown in figure 7 for 1000 and 6000 rpm. The pressure pattern at the end was essentially the same for the speed range investigated (1000 to 6000 rpm) except that the results for 5000 rpm (not shown) and 6000 rpm start to show a slight shortening of the end-effect length. In all cases, the end-effect length was approximately equal to one-half the groove width. This suggests that end-effect length could be taken equal to one-half groove width without significant error. The pressure decay

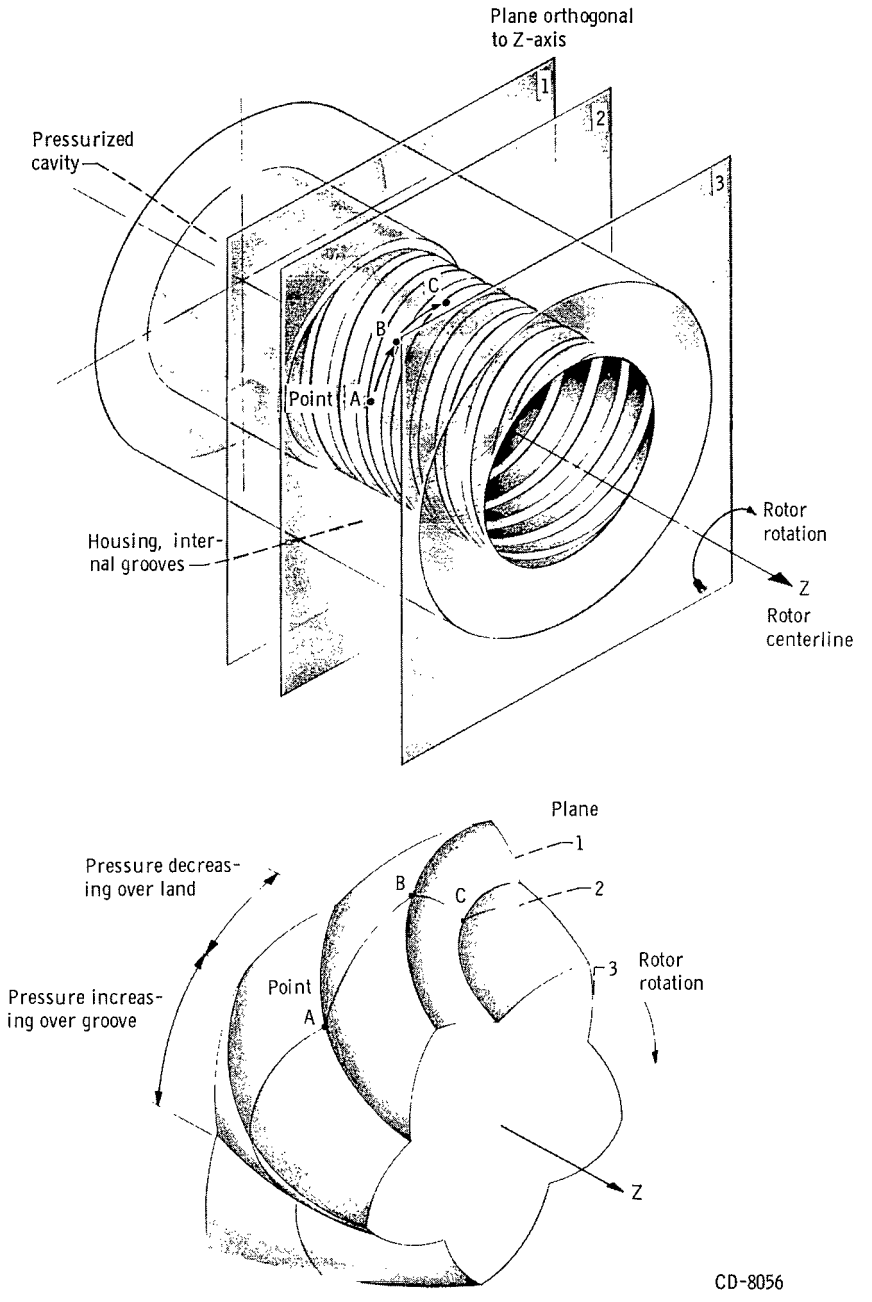

Figure 5. - Isometric representation of viscoseal and pressure patterns.

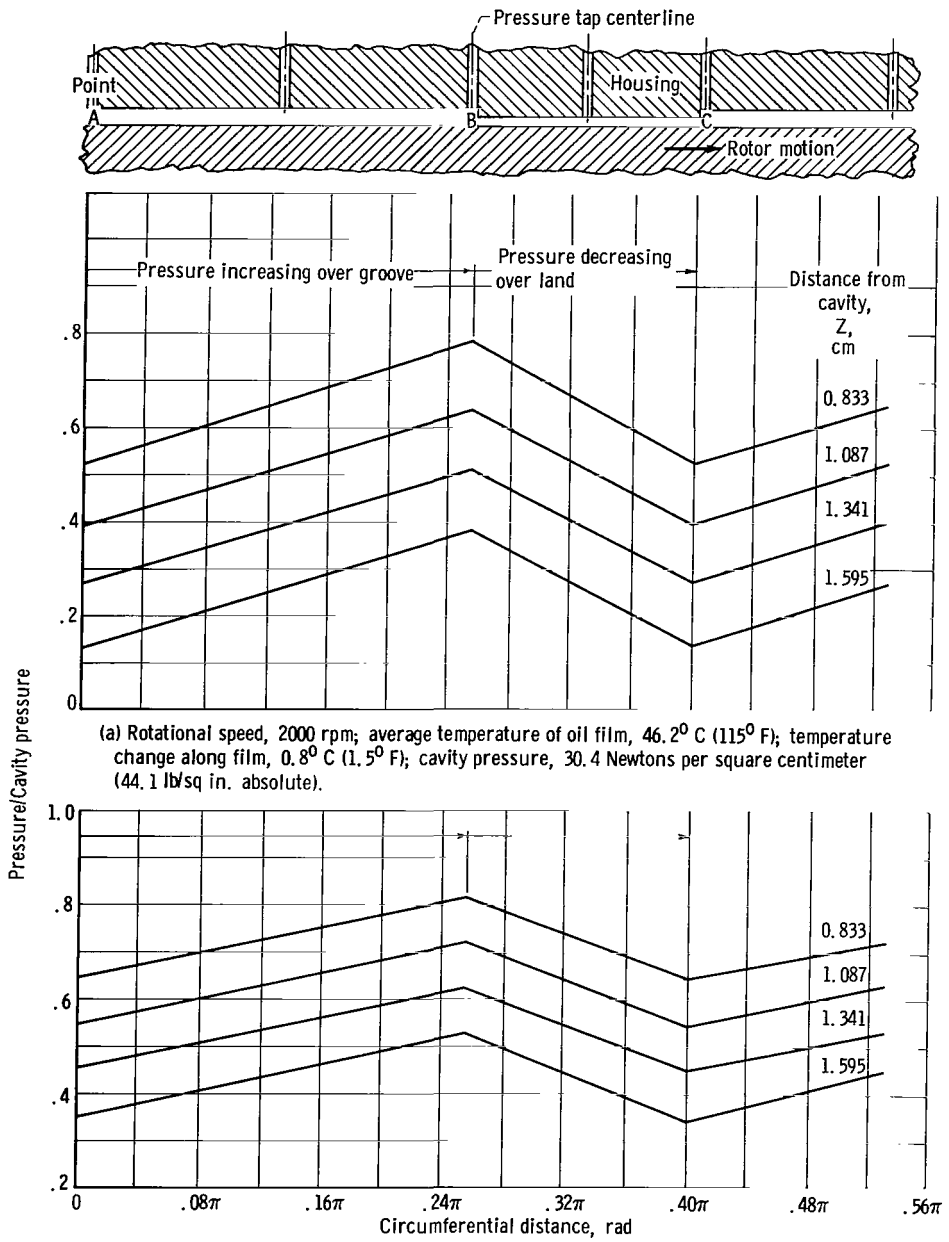

(a) Rotational speed, 2000 rpm; average temperature of oil film, 46.2° C (115° F); temperature change along film, 0.8° C (1.5° F); cavity pressure, 30.4 Newtons per square centimeter (44.1 lb/sq in. absolute).

(b) Rotational speed, 4000 rpm; average temperature of oil film, 58.9° C (138° F); temperature change along film, 2.2° C (4° F); cavity pressure, 41.5 Newtons per square centimeter (60.2 lb/sq in. absolute).

Figure 6. - Pressure gradients on planes orthogonal to z axis centerline.

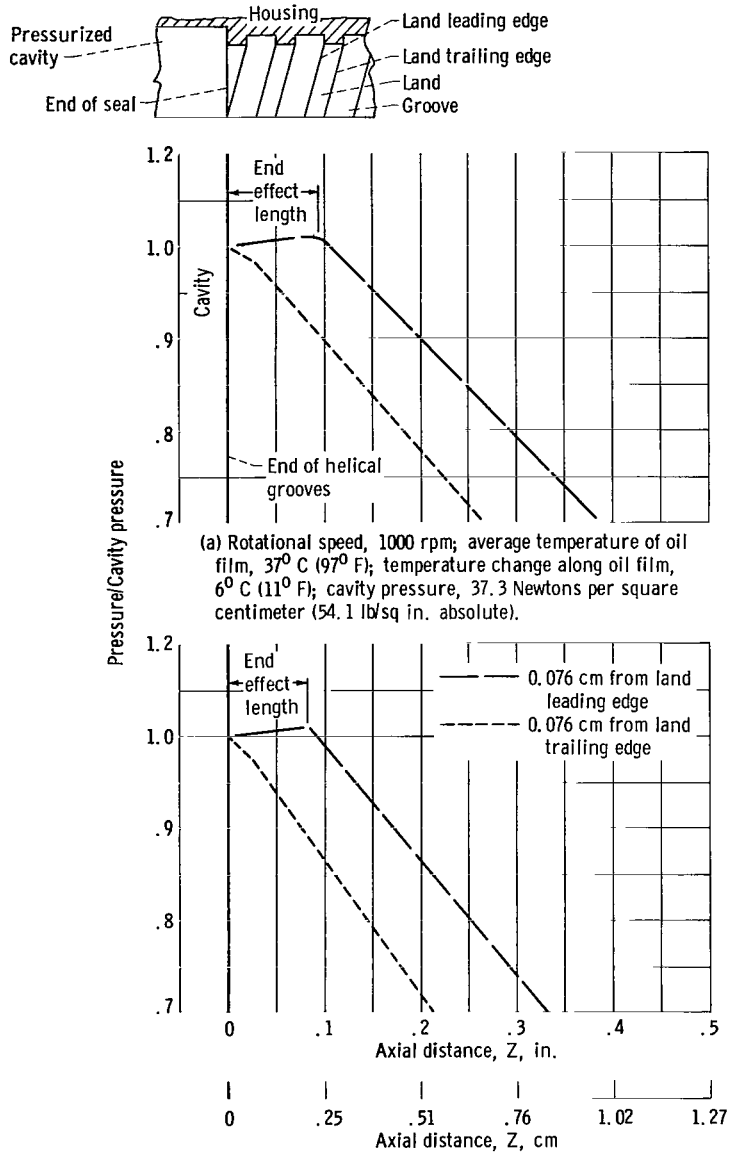

(a) Rotational speed, 1000 rpm; average temperature of oil film, 37° C (97° F); temperature change along oil film, 6° C (11° F); cavity pressure, 37.3 Newtons per square centimeter (54.1 lb/sq in. absolute).

(b) Rotational speed, 6000 rpm; average temperature of oil film, 56° C (132° F); temperature change along oil film, 11° C (19° F); cavity pressure, 55.6 Newtons per square centimeter (80.6 lb/sq in. absolute).

Figure 7. - Axial pressure gradients near helical groove edges with grooves in direct communication with pressurized cavity.

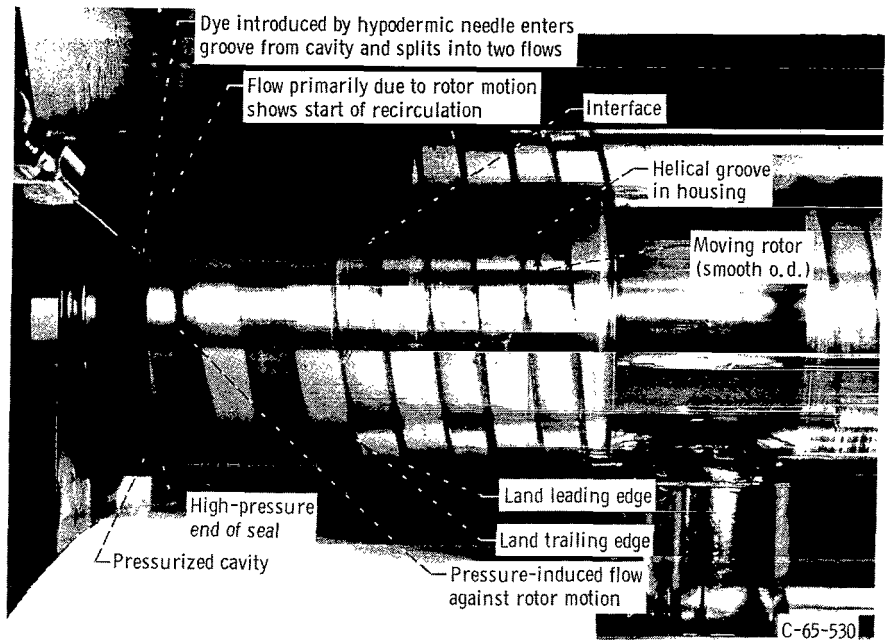

Figure 8. - End effect in model demonstrating fluid recirculation between cavity and groove.

within the groove is due to the equalization of the land leading- and trailing-edge pressure, since a common pressure must exist in the cavity. Figure 8 shows the flow pattern at the high-pressure end of the seal, which gives evidence of the pressure equalization process. Considerable inflow from the cavity is apparent in the dye motion.

Figure 9 gives a comparison of end-effect pressure distribution with and without a dam blocking groove communication with the pressurized cavity. When a short dam 0.076 centimeter (0.030 in.) long was employed, the land leading-edge pressure did not decay at the high-pressure end of the seal. It should be noted that, for equal cavity pressures, the seal with an end dam provides a shorter wetted-seal length because the end effect, or ineffective length, is eliminated. The radial clearance between dam and rotor was the same as that between land and rotor. No attempt was made to arrive at an optimum dam length; when the dam length was reduced to 0.038 centimeter (0.015 in.), however, a decay in pressure at the land leading edge was noted. Preliminary experiments using water indicated dam lengths to 0.380 centimeter (0.150 in.) did not eliminate the end effect.

Axial-Pressure Gradients

Figure 10 shows the pressure gradients that exist along the groove edges and at the midgroove and midland positions. Data taken at 3000 and 4000 rpm are shown. In all cases, the pressure gradients along the groove edges and at the midgroove and midland

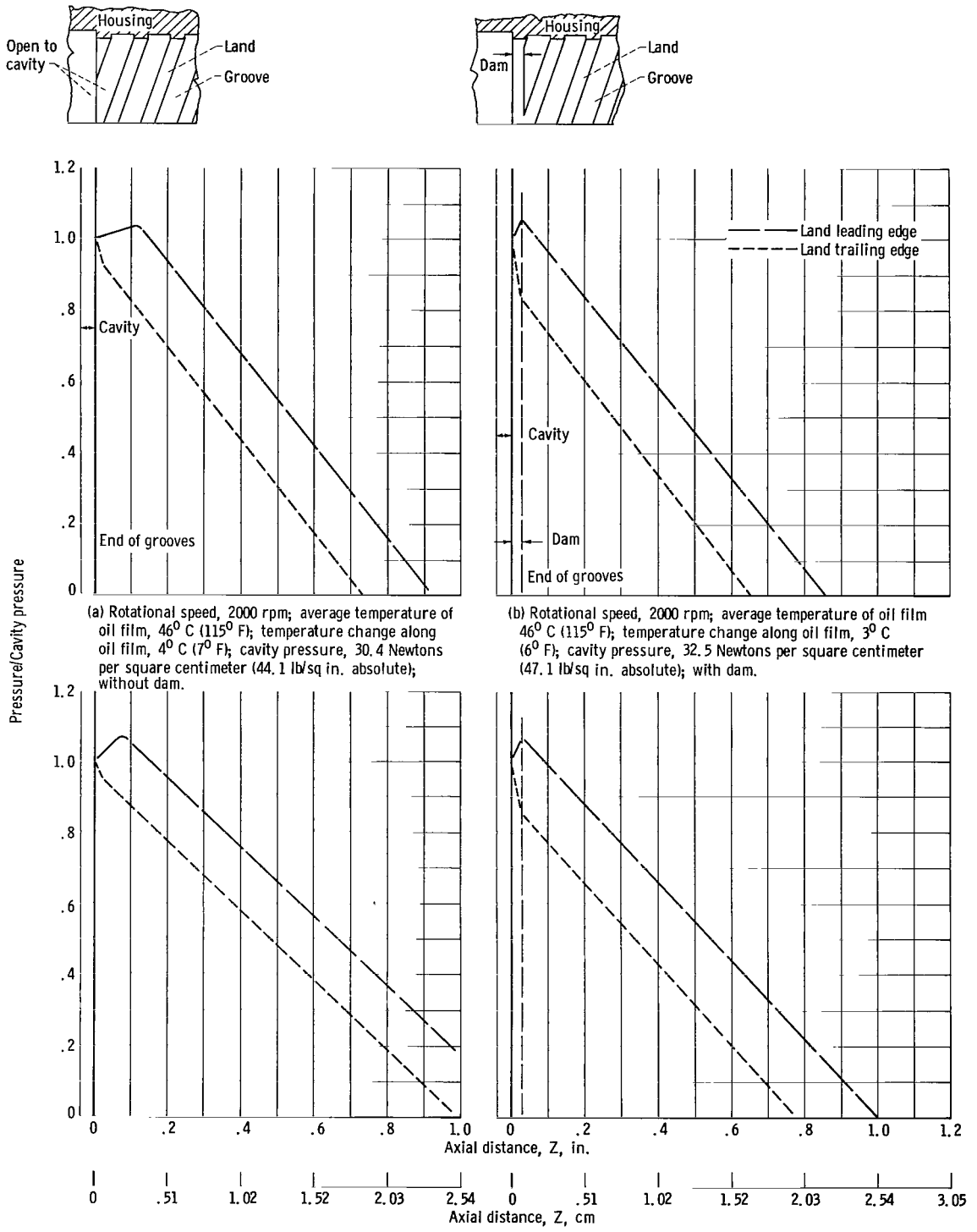

(a) Rotational speed, 2000 rpm; average temperature of oil film, 46° C (115° F); temperature change along oil film, 4° C (7° F); cavity pressure, 30.4 Newtons per square centimeter (44.1 lb/sq in. absolute); without dam.

(b) Rotational speed, 2000 rpm; average temperature of oil film 46° C (115° F); temperature change along oil film, 3° C (6° F); cavity pressure, 32.5 Newtons per square centimeter (47.1 lb/sq in. absolute); with dam.

(c) Rotational speed, 5000 rpm; average temperature of oil film, 64° C (148° F); temperature change along oil film, 3° C (5° F); cavity pressure, 40.5 Newtons per square centimeter (58.8 lb/sq in. absolute); without dam.

(d) Rotational speed, 5000 rpm; average temperature of oil film, 64° C (148° F); temperature change along oil film, 6° C (10° F); cavity pressure, 37.0 Newtons per square centimeter (53.6 lb/sq in. absolute); with dam.

Figure 9. - Axial pressure gradients along helical groove edges.

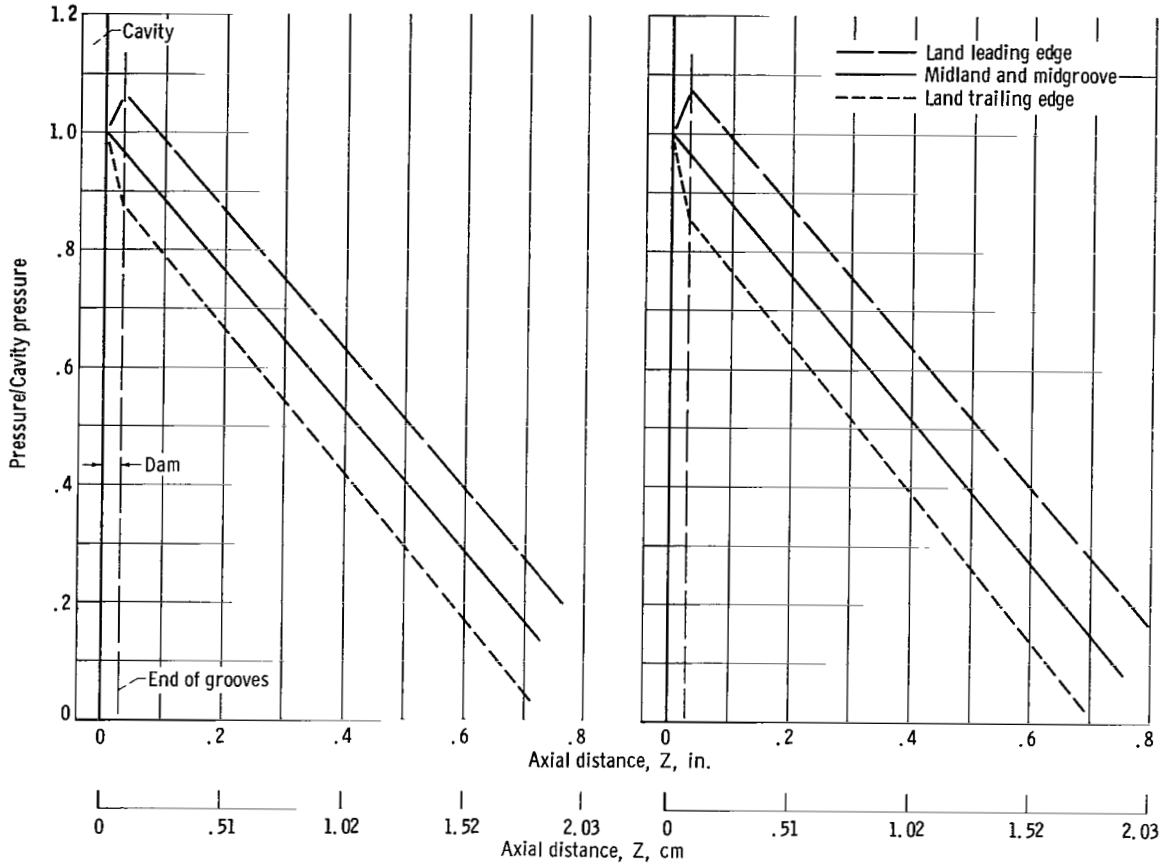

(a) Rotational speed, 3000 rpm; average temperature of oil film, 52° C (126° F); temperature change along oil film, 3° C (6° F); cavity pressure, 34.5 Newtons per square centimeter (50.1 lb/sq in. absolute).

(b) Rotational speed, 4000 rpm; average temperature of oil film, 57° C (134° F); temperature change along oil film, 4° C (8° F); cavity pressure, 36.7 Newtons per square centimeter (53.2 lb/sq in absolute).

Figure 10. - Axial pressure gradients with dam blocking groove communication with pressurized cavity.

positions are linear and have a common slope which is defined by the pressure generation equation

$$\frac{P}{L} = \frac{6U\mu G}{c^2}$$

The end effect and interface length, which are part of the overall seal length considerations, are not included in this pressure generation equation and must be accounted for separately. In the case of direct communication of grooves to the pressurized cavity, the pressure gradient can be considered to apply to the pressure along the land trailing edge without significant error (see fig. 11(a)). The actual wetted length is then obtained by adding the interface length, which was observed to be approximately equal to the axial width of one groove for the flow regime investigated (maximum Reynolds number in

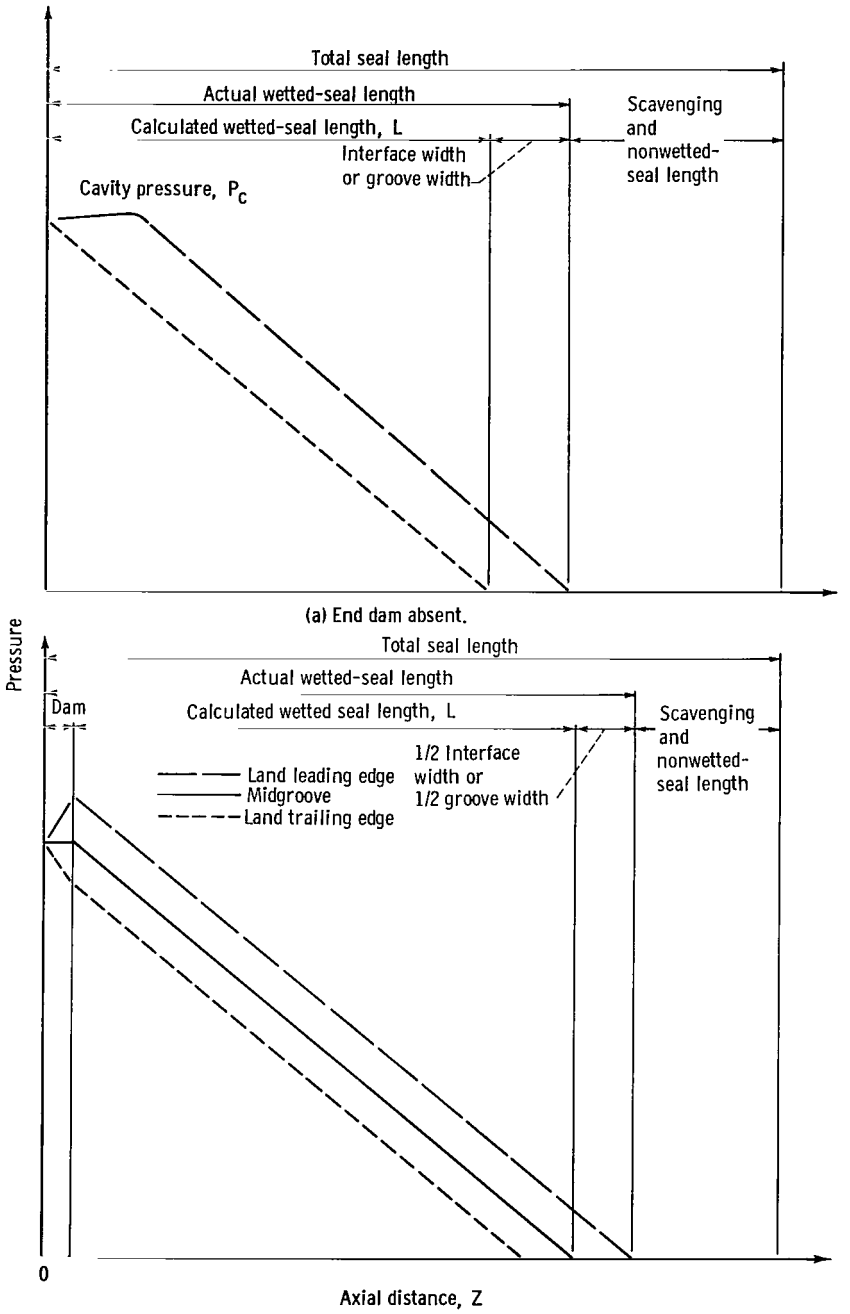

Figure 11. - Determination of seal length.

grooves was 300). In the case where the grooves are sufficiently blocked from direct communication with the cavity, extension of the midgroove pressure gradient intersects the cavity pressure. Therefore, the pressure generation equation can be considered to apply to the midgroove axial pressure gradient, and the actual wetted-seal length is obtained by adding the dam length and one-half of the interface length to the calculated seal length (see fig. 11(b)). It should be pointed out that a scavenging and nonwetted-seal length is also required in order to prevent the escape of fluid which breaks away from the interface. Values of dimensionless factor G (table I) were not investigated.

SUMMARY OF RESULTS

Pressure patterns were studied for a viscoseal in the laminar-flow regime with a mineral oil, and the following results were obtained:

1. For the condition of helical grooves in direct communication with the pressurized cavity, the end effect is evidenced by a decay of land leading-edge pressure. For operation with oil this end effect, or ineffective length, was eliminated by using a dam to block the communication of the grooves with the pressurized cavity.

2. No significant change in end-effect length was noted over the speed range investigated (Reynolds numbers of 50 to 300).

3. Circumferential pressure gradients in the plane of rotation (plane orthogonal to z-axis) increase linearly across the groove and decrease linearly across the land. This pressure pattern repeats for each groove-land pair and provides a saw-tooth pressure profile around the circumference.

4. Actual wetted-seal length can be obtained by using the theoretical pressure generation equation to define (a) the pressure gradient along the land trailing edge, in the case of direct communication between grooves and cavity, to which must be added the interface axial length and (b) the pressure gradient along the midgroove position, in the case where the grooves are sufficiently blocked from direct communication with the cavity, to which must be added the dam length and one-half the interface length.

Lewis Research Center
National Aeronautics and Space Administration
Cleveland, Ohio, August 13, 1965.

REFERENCES

1. Billet, A. B.: Hydraulic Sealing in Space Environments. Proceedings of the Second International Conference on Fluid Sealing, Apr. 1964. British Hydromechanics Research Association, 1964, pp. C2-17 - C2-36.

2. Bisson, Edmond E.; and Anderson, William J.: Advanced Bearing Technology. NASA SP-38, 1964, p. 461.

3. Rowell, H. S.; and Finlayson, D.: Screw Viscosity Pumps. Engineering, vol. 114, Nov. 1922, pp. 606-607.

4. Rowell, H. S.; and Finlayson, D.: Screw Viscosity Pumps. Engineering, vol. 126, Aug. 1928, pp. 249-250.

5. Rowell, H. S.; and Finlayson, D.: Screw Viscosity Pumps. Engineering, vol. 126, Sept. 1928, pp. 385-387.

6. Rogowsky, Z.: Mechanical Principles of the Screw Extrusion Machine. Engineering, vol. 162, Oct. 1946, pp. 358-360.

7. Strub, R. A.: Spindle Drag Pump. Machine Design, vol. 25, July 1953, pp. 149-151.

8. Pigott, W. T.: Pressures Developed by Viscous Materials in the Screw Extrusion Machine. Trans. ASME, vol. 73, Oct. 1951, pp. 947-955.

9. Members of the Polychemicals Department, E. I. duPont de Nemours and Co.: Theory of Extrusion. Ind. Eng. Chem., vol. 45, May 1953, pp. 969-993.

10. Eccher, Silvio; and Valentinotti, Aldo: Experimental Determination of Velocity Profiles in an Extruder Screw. Ind. Eng. Chem., vol. 50, no. 5, May 1958, pp. 829-836.

11. Griffith, R. M.: Fully Developed Flow in Screw Extruders. Ind. Eng. Chem. Fundamentals, vol. 1, no. 3, Aug. 1962, pp. 180-187.

12. Squires, P. H.: Screw Extrusion - Flow Patterns and Recent Theoretical Developments. SPE Trans., vol. 4, no. 1, Jan. 1964, pp. 7-16.

13. Boon, E. F.; and Tal, S. E. (R. Presser, trans.): Hydrodynamic Seal for Rotating Shafts. Rep. DEG.-Inf.-Ser.-13, United Kingdom Atomic Energy Authority, 1961.

14. McGrew, J. M.; and McHugh, J. D.: Analysis and Test of the Screw Seal in Laminar and Turbulent Operation. J. Basic Eng., Trans. ASME, Ser. D, vol. 87, no. 1, Mar. 1965, pp. 153-162.

15. Zotov, V. A.: Research on Helical Groove Seals. Russ. Eng. J. English Transl., vol. 10, Oct. 1959, pp. 3-7.

16. Asanuma, T.: Studies on the Sealing Action of Viscous Fluids. Paper A3, International Conference on Fluid Sealing, Apr. 1961.

17. Lessley, R. L.; and Hodgson, J. N.: Low-Leakage Dynamic Seal-to-Space. Paper 65-GTP-14, Am. Soc. Mech. Engrs., Feb. 1965.

18. Muijderman, E. A.: Spiral Groove Bearings. Philips Res. Rept. Suppl. 1964, no. 2.

19. Pinkus, Oscar; and Sternlicht, Beno: Theory of Hydrodynamic Lubrication. McGraw-Hill Book Co., 1961.

20. Whipple, R. T. P.: The Inclined Groove Bearing. Rep. AERE-T/R-622(Rev.), Research Group, Atomic Energy Research Establishment, United Kingdom Atomic Energy Authority, 1958.

3/18/85

"The aeronautical and space activities of the United States shall be conducted so as to contribute . . . to the expansion of human knowledge of phenomena in the atmosphere and space. The Administration shall provide for the widest practicable and appropriate dissemination of information concerning its activities and the results thereof."

—NATIONAL AERONAUTICS AND SPACE ACT OF 1958

NASA SCIENTIFIC AND TECHNICAL PUBLICATIONS

TECHNICAL REPORTS: Scientific and technical information considered important, complete, and a lasting contribution to existing knowledge.

TECHNICAL NOTES: Information less broad in scope but nevertheless of importance as a contribution to existing knowledge.

TECHNICAL MEMORANDUMS: Information receiving limited distribution because of preliminary data, security classification, or other reasons.

CONTRACTOR REPORTS: Technical information generated in connection with a NASA contract or grant and released under NASA auspices.

TECHNICAL TRANSLATIONS: Information published in a foreign language considered to merit NASA distribution in English.

TECHNICAL REPRINTS: Information derived from NASA activities and initially published in the form of journal articles.

SPECIAL PUBLICATIONS: Information derived from or of value to NASA activities but not necessarily reporting the results of individual NASA-programmed scientific efforts. Publications include conference proceedings, monographs, data compilations, handbooks, sourcebooks, and special bibliographies.

Details on the availability of these publications may be obtained from:

SCIENTIFIC AND TECHNICAL INFORMATION DIVISION

NATIONAL AERONAUTICS AND SPACE ADMINISTRATION

Washington, D.C. 20546